HHS Public Access

Author manuscript

Nat Mater. Author manuscript; available in PMC 2014 December 01.

Published in final edited form as:

Nat Mater. 2014 June ; 13(6): 599–604. doi:10.1038/nmat3945.

Hippo/YAP-mediated rigidity-dependent motor neuron differentiation of human pluripotent stem cells

Yubing Sun[1], **Koh Meng Aw Yong**[1], **Luis G. Villa-Diaz**[2,3], **Xiaoli Zhang**[4], **Weiqiang Chen**[1], **Renee Philson**[5], **Shinuo Weng**[1], **Haoxing Xu**[4], **Paul H. Krebsbach**[2,3,5], and **Jianping Fu**[1,5,*]

[1]Department of Mechanical Engineering, University of Michigan, Ann Arbor, Michigan, USA

[2]Department of Biologic and Materials Sciences, University of Michigan, Ann Arbor, Michigan, USA

[3]Biointerfaces Institute, University of Michigan, Ann Arbor, Michigan, USA

[4]Department of Molecular, Cellular, and Developmental Biology, University of Michigan, Ann Arbor, Michigan, USA

[5]Department of Biomedical Engineering, University of Michigan, Ann Arbor, Michigan, USA

Abstract

Our understanding of the intrinsic mechanosensitive properties of human pluripotent stem cells (hPSCs), in particular the effects that the physical microenvironment has on their differentiation, remains elusive[1]. Here, we show that neural induction and caudalization of hPSCs can be accelerated by using a synthetic microengineered substrate system consisting of poly(dimethylsiloxane) micropost arrays (PMAs) with tunable mechanical rigidities. The purity and yield of functional motor neurons (MNs) derived from hPSCs within 23 days of culture using soft PMAs were improved more than 4- and 10-fold, respectively, compared to coverslips or rigid PMAs. Mechanistic studies revealed a multi-targeted mechanotransductive process involving Smad phosphorylation and nucleocytoplasmic shuttling, regulated by rigidity-dependent Hippo-YAP activities and actomyosin cytoskeleton integrity and contractility. Our findings suggest that substrate rigidity is an important biophysical cue influencing neural induction and subtype specification, and that microengineered substrates can thus serve as a promising platform for large-scale culture of hPSCs.

*Correspondence should be addressed to J. F. (jpfu@umich.edu).

COMPETING FINANCIAL INTERESTS

The authors declare no competing financial interests.

AUTHOR CONTRIBUTIONS

Y.S. and J.F. designed experiments; Y.S. performed *in vitro* differentiation experiments and Western blotting; K.M.A.Y., L.G.V-D., and Y.S. generated and analyzed gene expression data; K.M.A.Y. and Y.S. performed siRNA transfection; X.Z. performed electrophysiology measurements; L.G.V-D. derived hiPSCs; W.C. fabricated silicon masters; S.W. developed image processing program; Y.S., L.G.V-D., R.P., H.X., P.H.K., and J.F. analyzed data and wrote the manuscript; J.F. supervised the project. All authors edited and approved the final manuscript.

Human pluripotent stem cells (hPSCs) including human embryonic stem cells (hESCs) and induced pluripotent stem cells (hiPSCs) are a promising resource for regenerating complex neural tissues, including motor neurons (MNs)[2–3]. However, poorly defined culture conditions and inefficient protocols for derivation of MNs from hPSCs have hindered their use. Current hPSC-based MN differentiation relies on soluble morphogens including sonic hedgehog (SHH) and retinoic acid (RA) to direct MN specification. Because morphogenesis during embryonic development occurs through dynamic modulation of extracellular physical signals, matrix rigidity is likely to be important for the differentiation and functional maturation of neural subtypes from hPSCs. Here we investigated intrinsic mechanosensitive properties of hPSCs and determined how they could be leveraged to improve production of functional MNs using a synthetic, micromolded poly(dimethylsiloxane) (PDMS) micropost array (PMA) system (Supplementary Fig. 1 and **Methods**), which has a uniform surface geometry and different post heights to modulate substrate rigidity independent of effects on adhesion and other material surface properties[4].

The influence of substrate rigidity on neural induction of hPSCs was assessed using vitronectin-coated coverslips (with bulk modulus $E = 10^4$ kPa) and PMAs with a broad range of rigidities (E = 1.0–1,200 kPa). hESCs were seeded at 20,000 cells cm^{-2} on coverslips and PMAs in growth medium. After 24 hr, hESCs were switched to neural induction medium containing the dual Smad inhibitors, SB 431542 (SB, TGF-β inhibitor) and LDN 193189 (LDN, BMP4 inhibitor), to promote neural induction (Fig. 1a)[3]. No significant difference in cell attachment was observed between coverslips and PMAs of different rigidities (not shown). On coverslips and PMAs with E = 1,200 kPa (rigid PMAs), hESCs spread to form monolayers, whereas on PMAs with $E \leq 5.0$ kPa (soft PMAs), hESCs spontaneously migrated toward each other to form compact clusters. Cell spreading and nucleus size of hESCs were significantly reduced on soft PMAs relative to on coverslips or rigid PMAs (referred to henceforth as controls; Supplementary Fig. 2a–c). Notably, within 24 hr, 22.3% ± 6.2% of hESCs on soft PMAs had differentiated, indicated by loss of Oct4 (pluripotency-associated transcription factor) expression, whereas only 4.9% ± 1.0% (coverslip) and 3.9% ± 0.4% (rigid PMA) of hESCs on controls started differentiating (Supplementary Fig. 2d).

Expression of the early neuroectodermal differentiation marker, Pax6, was used to monitor neural induction. On soft PMAs, $Pax6^+$ neuroepithelial cells (NEs) were detected as early as day 4, and reached 95.1% ± 2.1% by day 8. In contrast, on controls, $Pax6^+$ NEs appeared at day 6 and constituted only 28.2% ± 10.8% (coverslip) and 33.4% ± 7.2% (rigid PMA) of total cells at day 8, respectively (Fig. 1b,c)[5]. Immunoblots revealed higher Pax6 and Sox1 (neuroectodermal transcription factor) protein expression by hESCs on soft PMAs relative to controls (Fig. 1d). Paralleling definitive neural stem cells in mouse embryos[6], $Pax6^+$ NEs derived from soft PMAs were responsive to bFGF and readily formed polarized neural tube-like rosettes, while the controls did not (Supplementary Fig. 3). A screening assay revealed a threshold of PMA rigidity E for neural induction: $E \leq 5$ kPa had a potent effect, whereas $E \geq 14$ kPa did not (Supplementary Fig. 4).

Two sets of PMAs with different post diameters but matching effective moduli E were compared, with results indicating that neural induction by soft PMAs was not sensitive to

micropost geometries (Supplementary Fig. 5). By modulating the PDMS curing agent to base monomer ratio (1:10–1:100), flat featureless PDMS surfaces with different bulk moduli *E* (0.5 kPa–2.5 MPa) were generated and assayed for neural induction. At day 6, $Pax6^+$ NEs constituted 32.5% ± 3.3% (1:70 PDMS, *E* = 5 kPa) and 27.7% ± 4.9% (1:100 PDMS, *E* = 0.5 kPa) of cells on soft, flat PDMS surfaces, respectively, in contrast to 14.3% ± 2.5% (coverslip) and 14.3% ± 1.8% (1:10 PDMS, *E* = 2.5 MPa) on controls (Supplementary Fig. 6). Noticeably, neural induction by soft, flat PDMS surfaces was not as drastic as soft PMAs, possibly owing to their viscoelastic nature, different from the elastic PMAs.

Temporal mRNA expression of pluripotency markers (*NANOG* and *SOX2*) and neuroectodermal markers (*PAX6*, *SOX1*, and *TUJ-1*) was quantified using qRT-PCR. Soft PMAs accelerated disruption of the transcriptional circuitry maintaining pluripotency, while promoting neuroectodermal gene expression (Supplementary Fig. 7). Experiments with another hESC line (CHB-10) and a hiPSC line derived from human foreskin fibroblasts showed that at day 6, $Pax6^+$ NEs constituted 60.8% ± 1.1% (CHB-10) and 78.8% ± 5.8% (hiPSCs) of cells on soft PMAs, respectively, in contrast to 23.2% ± 3.0% (CHB-10) and 24.5% ± 1.8% (hiPSCs) on rigid PMAs (Supplementary Fig. 8).

Treatment of hESCs with both Smad inhibitors led to $Pax6^+$ NEs, as well as $Pax6^-$ cells co-expressing neural crest (NC) markers AP2, p75, and HNK-1 (Fig. 1b and Supplementary Fig. 9)[3]. At day 8, 18.7% ± 5.3% and 18.1% ± 3.6% of cells were $AP2^+$ on coverslips and rigid PMAs, respectively. Strikingly, only 1.1% ± 0.5% of cells were $AP2^+$ on soft PMAs (Fig. 1b). Similar reductions in $p75^+$ and $HNK\text{-}1^+$ NCs were observed on soft PMAs (Supplementary Fig. 9). Paralleling the effects of substrate rigidity, manipulation of the concentration of the BMP4 inhibitor, LDN, altered the ratio of $Pax6^+$ NEs to $Pax6^-/AP2^+$ NCs. Increasing LDN levels promoted differentiation toward $Pax6^+$ NEs, whereas LDN's absence favored NC differentiation (Fig. 1e).

To induce functional neurons, NEs require anterior/posterior and dorsal/ventral patterning cues[2,7]. When the caudalization factor, RA, was added to neural induction medium from day 4, the posterior genes, *HOXB1*, *HOXB4,* and *HOXC8* were significantly upregulated, whereas *OTX2*, an anterior identity gene, was suppressed (Supplementary Fig. 10a,b). Surprisingly, soft PMAs promoted *HOXB1*, *HOXB4*, and *HOXC8* expression in the absence of RA (Supplementary Fig. 10b). Although RA's effects exceeded those of soft PMAs on OTX2, HOXB1, or HOXB4 expression, expression of *HOXB4* and *HOXC8* remained responsive to varying substrate rigidity in the presence of RA, suggesting an additive effect of substrate rigidity on neural caudalization. Otx2 and HoxB4 protein expression levels confirmed the effect of soft PMAs on promoting neural patterning and specification of posterior identity (Supplementary Fig. 10c,d).

We next examined whether the ventralization factor, Purmorphamine (Pur), could induce MNs from caudalized NEs derived from soft PMAs, using oligodendrocyte transcription factor 2 (Olig2) as a MN marker. When NEs were cultured continuously for an additional 8 d in the presence of Pur and RA, 65% ± 6.3% of cells on soft PMAs became $Olig2^+$, whereas only 7.9% ± 1.3% of cells were $Olig2^+$ on rigid PMAs (Supplementary Fig. 11). In

the absence of RA, 19.3% ± 1.7% of cells on soft PMAs became Olig2$^+$, whereas on rigid PMAs only 3.5% ± 1.6% of cells were Olig2$^+$.

Because soft PMAs accelerate neural induction and caudalization, we investigated whether functional MN production could be expedited using soft PMAs. hESCs were cultured on vitronectin-coated coverslips and PMAs for 16 d to allow neural induction and caudalization prior to passage onto poly-l-ornithine/laminin/fibronectin-coated coverslips and treatment with MN maturation medium containing neurotrophic factors BDNF and IGF-1 for an additional 14 d (Fig. 2a). At day 23, 18.5% ± 0.6%, 11.4% ± 0.3%, and 12.0% ± 1.1% of cells derived from soft PMAs became Tuj1$^+$ (neuronal form of tubulin), Isl1$^+$ (MN-associated transcription factor), and HB9$^+$ (MN-specific transcription factor), respectively. In contrast, Tuj1$^+$, Isl1$^+$, and HB9$^+$ cells derived from coverslips constituted 8.0% ± 0.7%, 2.6% ± 0.6%, and 2.6% ± 0.5% of total cells, respectively (Fig. 2b,c). Similarly, only 6.3% ± 0.7%, 2.2% ± 0.3%, and 2.0% ± 0.2% of cells derived from rigid PMAs were Tuj1$^+$, Isl1$^+$, and HB9$^+$, respectively (Fig. 2b,c). 62.6% ± 1.1% of Tuj1$^+$ cells derived from soft PMAs co-expressed Isl1, whereas on controls only 33.3% ± 6.2% (coverslip) and 33.5% ± 8.1% (rigid PMA) of Tuj1$^+$ cells were Isl1$^+$ (Fig. 2c). Notably, significantly more soft PMA-derived cells expressed choline acetyltransferase (ChAT), an enzyme catalyzing the formation of neurotransmitter acetylcholine, at day 30, compared to controls (Fig. 2b). The purity of MNs, defined as the percentage of HB9$^+$ cells, from soft PMAs was thus improved about 4.6-fold, compared to controls (Fig. 2c). Furthermore, subculture of MN progenitors derived from soft PMAs led to 7.5-, 11.7-, and 12.9-fold increases in the numbers (and thus yields) of Tuj1$^+$, Isl1$^+$, and HB9$^+$ cells, respectively (Fig. 2d).

We next evaluated action potentials (APs) for functional MNs derived at day 30 from soft PMAs using whole-cell recording (**Methods**). Among 27 cells recorded, 12 generated APs with an average amplitude > 65 mV and were considered functionally mature[8]. Another 5 cells fired APs with the average amplitude < 65 mV. Nine displayed spontaneous APs with an average amplitude of 85.3 mV and a half-height width of 2.5 ms (Fig. 2e). When injected with depolarizing currents, 15 cells displayed tonic firing activities with an average first spike amplitude of 71.7 mV (Fig. 2f). MNs can decrease firing rates responding to constant stimuli, a phenomenon called spike frequency adaption (SFA)[9]. Here, 6 of 12 “mature” MNs displayed SFA with a depolarizing current (Fig. 2g). Moreover, post-inhibitory rebound (PIR, depolarization and/or spiking following a release from hyperpolarization) was observed in 6 MNs (Fig. 2h). These data suggest that MNs derived from soft PMAs display electrophysiological activities comparable to those from primary neurons *in vivo*[8]. In comparison, hPSCs require up to 50 days under conventional differentiation conditions for complete functional maturation into a MN[10–11].

To examine whether rigidity-mediated MN production might depend on specific ventralizing and neurotrophic factors, additional 23-day and 35-day MN differentiation assays were conducted using SHH for patterning and ventralization and neurotrophic factors BDNF, GDNF, CNTF, and IGF-1 for terminal differentiation (Supplementary Fig. 12 and Supplementary Fig. 13). For the 23-day assay, 32.8% ± 5.7% and 17.7% ± 1.7% of cells derived from soft PMAs became Tuj1$^+$ and HB9$^+$, respectively, at day 23 (Supplementary Fig. 12b,c). In contrast, for controls, 14.6% ± 1.3% (coverslip) and 10.3% ± 2.5% (rigid

PMA) of cells were Tuj1$^+$, and 3.8% ± 0.4% (coverslip) and 3.0% ± 0.8% (rigid PMA) cells were HB9$^+$ (Supplementary Fig. 12b,c). The purity and total number (and thus yield) of HB9$^+$ MNs derived from soft PMAs were improved 4.6- and 12.9-fold, respectively, compared to controls (Supplementary Fig. 12c,d). Similarly, in the 35-day assay, the percentage of HB9$^+$ cells at day 35 improved from 7.3% ± 3.1% (coverslip) and 7.8% ± 1.2% (rigid PMA) to 47.7% ± 2.3% (soft PMA) (Supplementary Fig. 13b-d). The purity and yield of HB9$^+$ MNs derived from soft PMAs were increased 6.1- and 10-fold, respectively, compared to controls (Supplementary Fig. 13c,d).

Our data presented in Fig. 1 suggested a connection between mechanotransduction and inhibition of BMP signaling in hPSCs. Indeed, immunoblots substantiated an inhibitory role of soft PMAs on Smad1/5/8 phosphorylation (Fig. 3a). Phosphorylated Smads (phosphoSmads) require translocation to the nucleus for transcriptional activation[12]. YAP/TAZ, nuclear transducers in the canonical Hippo pathway, bind phosphoSmads and control their nucleocytoplasmic shuttling in hESCs[13]. In the Hippo pathway, Lats1/2 kinase phosphorylates YAP/TAZ, which in turn bind the scaffolding protein 14-3-3 to remain cytoplasmic[14]. YAP/TAZ-mediated nuclear accumulation of phosphoSmads is required for hESC pluripotency and its loss results in neuroectoderm differentiation[13]. A recent study also shows that YAP/TAZ are critical in mechanotransduction[15–16].

Supporting our hypothesis that YAP/TAZ-mediated nuclear accumulation of Smads regulates rigidity-dependent neural induction of hESCs, nuclear YAP/TAZ were observed in 95% ± 2.7% and 38.2% ± 1.6% of hESCs on rigid and soft PMAs, respectively (Fig. 3b,c). Rigidity-dependent subcellular localization of YAP/TAZ was maintained after 3 d of neural induction and coincided with nucleocytoplasmic shuttling of Smad 2/3 and Smad 1/5/8 (Fig. 3d). Co-localization of YAP/TAZ and phosphoSmad 1/5/8 was also observed before and after neural induction (Supplementary Fig. 14).

We next examined whether substrate rigidity regulates YAP/TAZ in hESCs in a Hippo-dependent manner. Immunoblots demonstrated that soft PMAs promoted YAP phosphorylation on serine 127 (ser^{127}), a key target of Lats1/2 kinase downstream of the Hippo pathway (Fig. 3e). Silencing of *Lats1* expression using siRNA suppressed YAP phosphorylation on ser^{127} (Supplementary Fig. 15). Notably, *Lats1* knockdown hESCs displayed a spread morphology on both rigid and soft PMAs, indicating loss of mechanosensory properties (Supplementary Fig. 15). Soft PMAs did not promote neural induction of *Lats1* knockdown hESCs (Fig. 3f,g), further supporting that Lats-mediated phosphorylation of YAP may relay mechanical signals exerted by substrate rigidity.

Adult mammalian cell studies suggest functional links between two major intracellular mechanotransductive components, Rho GTPase and the actomyosin cytoskeleton (CSK), and the Hippo-YAP pathway[16–19]. Indeed, hESCs cultured on rigid PMAs exhibited bundled actin microfilaments at cell peripheries, whereas actin microfilaments were diffusely distributed throughout cells on soft PMAs (Supplementary Fig. 16). hESCs were treated independently with Y27632 (inhibitor of Rho-associated kinase, or ROCK, a downstream effector of RhoA), which decreases actomyosin contractility while maintaining intact CSK structure; cytochalasin D (CytoD), an inhibitor of actin polymerization; or

lysophosphatidic acid (LPA), which stimulates RhoA and facilitates formation of actin microfilaments. Compared to controls, Y27632 promoted cytoplasmic localization of YAP/TAZ and significantly increased the percentage of $Pax6^+$ NEs on rigid, but not soft PMAs (Supplementary Fig. 17 and Fig. 3h–j). In contrast, LPA facilitated nuclear localization of YAP/TAZ and inhibited neural induction on both rigid and soft PMAs. Notably, CytoD treatment had a significant effect on YAP/TAZ translocation on both rigid and soft PMAs, and neural induction was significantly more efficient on soft PMAs without treatment, compared to that on rigid PMAs treated with Y27632 (Fig. 3h–j). These data are consistent with findings that ROCK inhibition facilitates neural differentiation of mouse ESCs and embryonal carcinoma stem cells[20–21], while LPA maintains hESC pluripotency[22–23].

Together, our studies suggest a putative multi-targeted mechanotransductive process in hPSCs where soft PMAs inhibit Smad phosphorylation while activating Lats, an actin-binding protein[24], during disassembly of actin microfilaments. This in turn phosphorylates YAP to prevent nuclear translocation of phosphoSmads and inhibit subsequent activation of Smad target genes (Supplementary Fig. 18).

The Hippo-YAP signaling pathway is highly conserved and under intense study given its importance in development and cancer. The current view implicates Hippo signaling regulated by cell polarity and adhesion proteins. Our data reveal functional crosstalk between Hippo-YAP signaling and the classic mechanotransductive components, Rho GTPase and the actomyosin CSK, in hPSCs. Other mechanosensory components, such as adhesion molecules including integrins and cadherins and cell morphology, may also regulate Hippo-YAP signaling in hPSCs. Supporting this view, increased internalization of integrins in mesenchymal stem cells on soft substrates represses Smad 1/5/8 phosphorylation and induces neurogenic differentiation[25]. Also, NIH/3T3 cell morphology regulates the Hippo pathway[16].

By combining dual Smad inhibition with PMAs, we generated high-yield and -purity functional MNs from hPSCs. PMAs are fully defined substrates that can be mass-produced for large-scale hPSC culture. We demonstrate that like many human adult stem cells[26–30], hPSCs are intrinsically mechanosensitive and substrate rigidity is an *in vitro* extracellular switch that directs NE *vs.* NC lineage decisions and anterior *vs.* posterior patterning. Mechanical properties of the extracellular matrix *in vivo* may act as a “mechanical organizer” synergizing with morphogens to direct neural plate specification and anterior-posterior axis formation during neurulation.

Supplementary Material

Refer to Web version on PubMed Central for supplementary material.

Acknowledgments

This work is supported by the National Science Foundation (CMMI 1129611 and CBET 1149401 to JF), the National Institutes of Health (1R21HL114011 to JF; 2R01DE016530-06 to PHK; R01NS062792 and R01AR060837 to HX), the American Heart Association (12SDG12180025 to JF), and the Department of Mechanical Engineering at the University of Michigan, Ann Arbor. The Lurie Nanofabrication Facility at the

University of Michigan, a member of the National Nanotechnology Infrastructure Network (NNIN) funded by the National Science Foundation, is acknowledged for support in microfabrication.

References

1. Discher DE, Mooney DJ, Zandstra PW. Growth factors, matrices, and forces combine and control stem cells. Science. 2009; 324:1673–1677. [PubMed: 19556500]
2. Li XJ, et al. Specification of motoneurons from human embryonic stem cells. Nat Biotechnol. 2005; 23:215–221. [PubMed: 15685164]
3. Chambers SM, et al. Highly efficient neural conversion of human ES and iPS cells by dual inhibition of Smad signaling. Nat Biotechnol. 2009; 27:275–280. [PubMed: 19252484]
4. Fu JP, et al. Mechanical regulation of cell function with geometrically modulated elastomeric substrates. Nature Methods. 2010; 7:733–736. [PubMed: 20676108]
5. Keung AJ, Asuri P, Kumar S, Schaffer DV. Soft microenvironments promote the early neurogenic differentiation but not self-renewal of human pluripotent stem cells. Integr Biol. 2012; 4:1049–1058.
6. Hitoshi S, et al. Primitive neural stem cells from the mammalian epiblast differentiate to definitive neural stem cells under the control of Notch signaling. Genes Dev. 2004; 18:1806–1811. [PubMed: 15289455]
7. Patani R, et al. Retinoid-independent motor neurogenesis from human embryonic stem cells reveals a medial columnar ground state. Nat Commun. 2011; 2:214. [PubMed: 21364553]
8. Bean BP. The action potential in mammalian central neurons. Nat Rev Neurosci. 2007; 8:451–465. [PubMed: 17514198]
9. Miles GB, Dai Y, Brownstone RM. Mechanisms underlying the early phase of spike frequency adaptation in mouse spinal motoneurones. J Physiol. 2005; 566:519–532. [PubMed: 15878947]
10. Karumbayaram S, et al. Human embryonic stem cell-derived motor neurons expressing SOD1 mutants exhibit typical signs of motor neuron degeneration linked to ALS. Dis Model Mech. 2009; 2:189–195. [PubMed: 19259395]
11. Hester ME, et al. Rapid and efficient generation of functional motor neurons from human pluripotent stem cells using gene delivered transcription factor codes. Mol Ther. 2011; 19:1905–1912. [PubMed: 21772256]
12. Derynck R, Zhang YE. Smad-dependent and Smad-independent pathways in TGF-β family signalling. Nature. 2003; 425:577–584. [PubMed: 14534577]
13. Varelas X, et al. TAZ controls Smad nucleocytoplasmic shuttling and regulates human embryonic stem-cell self-renewal. Nat Cell Biol. 2008; 10:837–848. [PubMed: 18568018]
14. Zhao B, et al. Inactivation of YAP oncoprotein by the Hippo pathway is involved in cell contact inhibition and tissue growth control. Genes Dev. 2007; 21:2747–2761. [PubMed: 17974916]
15. Dupont S, et al. Role of YAP/TAZ in mechanotransduction. Nature. 2011; 474:179–183. [PubMed: 21654799]
16. Wada K, et al. Hippo pathway regulation by cell morphology and stress fibers. Development. 2011; 138:3907–3914. [PubMed: 21831922]
17. Yu FX, et al. Regulation of the Hippo-YAP pathway by G-protein-coupled receptor signaling. Cell. 2012; 150:780–791. [PubMed: 22863277]
18. Calvo F, et al. Mechanotransduction and YAP-dependent matrix remodelling is required for the generation and maintenance of cancer-associated fibroblasts. Nat Cell Biol. 2013; 15:637–646. [PubMed: 23708000]
19. Zhao B, et al. Cell detachment activates the Hippo pathway via cytoskeleton reorganization to induce anoikis. Genes Dev. 2012; 26:54–68. [PubMed: 22215811]
20. Chang TC, et al. Rho kinases regulate the renewal and neural differentiation of embryonic stem cells in a cell plating density–dependent manner. PLoS ONE. 2010; 5:e9187. [PubMed: 20169147]
21. Krawetz RJ, et al. Inhibition of Rho kinase regulates specification of early differentiation events in P19 embryonal carcinoma stem cells. PLoS ONE. 2011; 6:e26484. [PubMed: 22140430]

22. Garcia-Gonzalo FR, Izpisua Belmonte JC. Albumin-associated lipids regulate human embryonic stem cell self-renewal. PLoS ONE. 2008; 3:e1384. [PubMed: 18167543]
23. Blauwkamp TA, et al. Endogenous Wnt signalling in human embryonic stem cells generates an equilibrium of distinct lineage-specified progenitors. Nat Commun. 2012; 3:1070. [PubMed: 22990866]
24. Visser-Grieve S, et al. Lats1 tumor suppressor is a novel actin-binding protein and negative regulator of actin polymerization. Cell Res. 2011; 21:1513–1516. [PubMed: 21808298]
25. Du J, et al. Integrin activation and internalization on soft ECM as a mechanism of induction of stem cell differentiation by ECM elasticity. Proc Natl Acad Sci USA. 2011; 108:9466–9471. [PubMed: 21593411]
26. Engler AJ, Sen S, Sweeney HL, Discher DE. Matrix elasticity directs stem cell lineage specification. Cell. 2006; 126:677–689. [PubMed: 16923388]
27. Connelly JT, et al. Actin and serum response factor transduce physical cues from the microenvironment to regulate epidermal stem cell fate decisions. Nat Cell Biol. 2010; 12:711–718. [PubMed: 20581838]
28. Gilbert PM, et al. Substrate elasticity regulates skeletal muscle stem cell self-renewal in culture. Science. 2010; 329:1078–1081. [PubMed: 20647425]
29. Holst J, et al. Substrate elasticity provides mechanical signals for the expansion of hemopoietic stem and progenitor cells. Nat Biotechnol. 2010; 28:1123–1128. [PubMed: 20890282]
30. Huebsch N, et al. Harnessing traction-mediated manipulation of the cell/matrix interface to control stem-cell fate. Nature Mater. 2010; 9:518–526. [PubMed: 20418863]

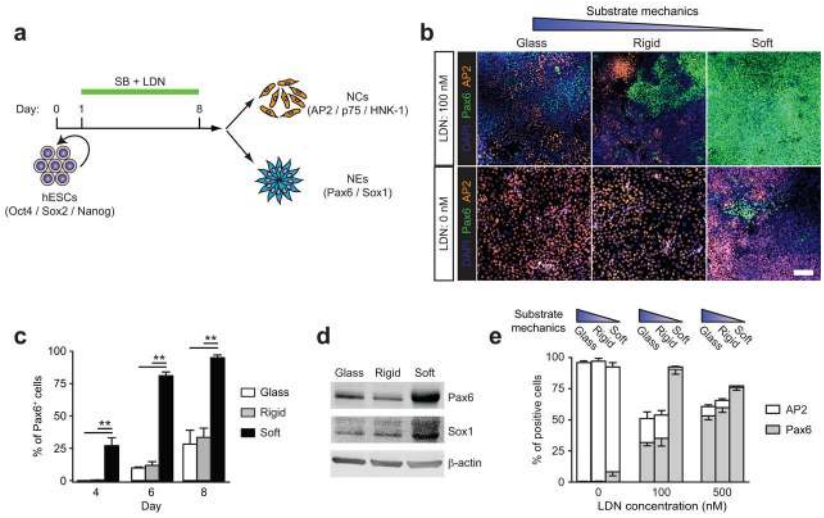

Figure 1.

Soft substrates promote neuroepithelial conversion while inhibiting neural crest differentiation of hESCs in a BMP4-dependent manner. (**a**) Schematic diagram showing experimental design of hESC neural induction. hESCs were cultured for 8 d in neural induction medium containing the dual Smad inhibitors, SB 431542 (SB, 10 μM) and LDN 193189 (LDN, 100 nM). (**b**) Representative immunofluorescence images showing $Pax6^+$ NEs and $AP2^+$ NCs after 8 d of culture with (*top*; 100 nM) or without (*bottom*) LDN on vitronectin-coated coverslips and rigid (E = 1,200 kPa) and soft (E = 5 kPa) PMAs. Scale bar, 100 μm. (**c**) Bar graph showing percentage of $Pax6^+$ NEs on coverslips and rigid and soft PMAs at day 4, 6, and 8. (**d**) Western blotting showing Pax6 and Sox1 expression levels in hESCs cultured for 8 d on coverslips and rigid and soft PMAs. (**e**) Bar plot showing percentages of $Pax6^+$ NEs and $AP2^+$ NCs at day 8 as a function of substrate rigidity and LDN concentration. Data represents the mean ± s.e.m with n = 3. P-values were calculated using one-way *ANOVA,* followed by Tukey post hoc analysis. *, $P < 0.05$; **, $P < 0.01$.

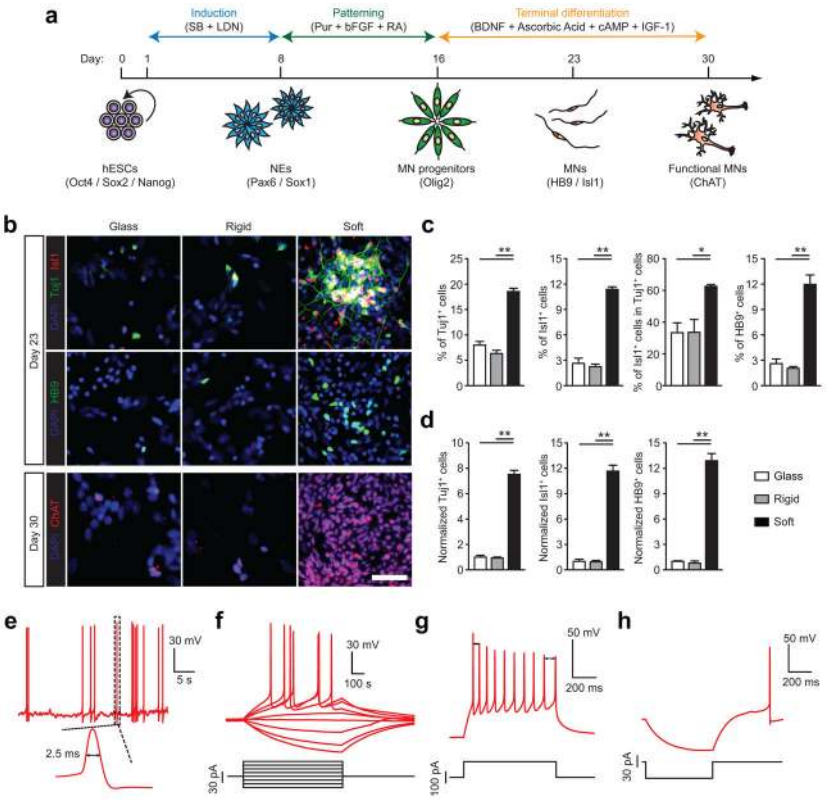

Figure 2.

Purity and yield of functional motor neurons (MNs) derived from hESCs are improved on soft substrates. (**a**) Schematic diagram showing experimental design for sequential neural induction, patterning, and functional maturation of MNs from hESCs. hESCs were cultured on vitronectin-coated coverslips and rigid (E = 1,200 kPa) and soft (E = 5 kPa) PMAs in neural induction medium containing the dual Smad inhibitors SB and LDN for 8 d and then in MN differentiation medium containing purmorphamine (Pur), basic fibroblast growth factor (bFGF), and retinoic acid (RA) for an additional 8 d. Putative MN progenitor cells collected at day 16 were transferred onto coverslips and cultured in MN maturation medium containing brain-derived neurotrophic factor (BDNF), ascorbic acid, cyclic adenosine monophosphate (cAMP), and insulin-like growth factor 1 (IGF-1) for another 14 d. (**b**) Representative immunofluorescence images showing Tuj1$^+$, Isl1$^+$, and HB9$^+$ cells at day 23 (*top*), and ChAT$^+$ cells at day 30 (*bottom*). Scale bar, 100 μm. (**c&d**) Bar plots showing percentages (**c**) and relative numbers (**d**) of Tuj1$^+$, Isl1$^+$, and HB9$^+$ cells at day 23 as a function of substrate rigidity. Data in **d** was normalized to values from coverslips. Data represents the mean ± s.e.m with $n \geq 3$. P-values were calculated using two-side unpaired student t-tests. *: $P < 0.05$; **: $P < 0.01$. (**e–h**) Electrophysiological characterization of functional MNs derived from soft PMAs at day 30 using whole-cell patch clamp. **e**: spontaneous action potential (AP) with resting membrane potential of −64.5 mV; **f**: voltage response to current step injection; **g**: instantaneous frequency change or spike frequency adaptation (SFA) evoked with positive current injection; **h**: post-inhibitory rebound (PIR) after hyperpolarizing current injection.

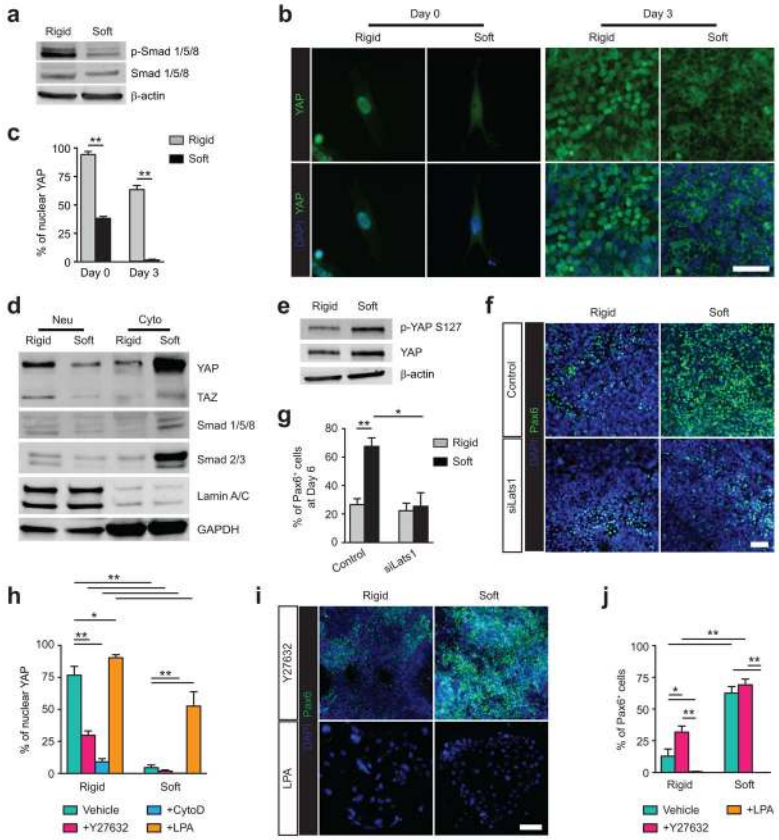

Figure 3.

Soft substrates promote hESC neuroepithelial conversion through a multi-targeted mechanotransductive process involving mechanosensitive Smad phosphorylation and nucleocytoplasmic shuttling regulated by rigidity-dependent Hippo-YAP activities and the actomyosin cytoskeleton (CSK). (**a**) Western blotting of total and phosphorylated Smad 1/5/8 (p-Smad 1/5/8) in hESCs cultured in neural induction medium for 3 d on rigid (E = 1,200 kPa) and soft (E = 5 kPa) PMAs. (**b&c**) Representative immunofluorescence images (**b**) and bar plot (**c**) showing rigidity-dependent subcellular localization of YAP in hESCs at day 0 and day 3. Scale bar in **b**, 50 μm. (**d**) Western blotting for YAP, TAZ, Smad 1/5/8, and Smad 2/3 in nuclear and cytoplasmic protein fractions from hESCs cultured for 3 d on rigid and soft PMAs. (**e**) Western blotting for phosphorylated YAP S127 (p-YAP S127) and YAP in whole cell lysates of hESCs after 3 d of culture on rigid and soft PMAs. (**f&g**) Representative immunofluorescence images (**f**) and bar plot (**g**) showing the percentage of Pax6$^+$ NEs derived from scramble control and *siLats1* knockdown hESCs after 6 d of culture on rigid and soft PMAs. Scale bar in **f**, 50 μm. (**h**) Bar graph showing the percentage of hESCs with nuclear localization of YAP after 3 d of culture with different drug supplementations, as indicated. (**i&j**) Representative immunofluorescence images (**i**) and bar plot (**j**) showing the percentage of Pax6$^+$ NEs derived from hESCs on rigid and soft PMAs after 6 d of culture with different drug supplementations, as indicated. Scale bar in **i**, 50 μm. In Western blots β-actin and GAPDH were used as protein loading controls and lamin A/C for nuclear fraction control. Data represents the mean ± s.e.m with $n \geq 3$. P-values in **c** & **g**

and **h** & **j** were calculated using two-side unpaired student *t*-tests and one way *ANOVA* followed by Tukey post hoc analysis, respectively. *, $P < 0.05$; **, $P < 0.01$.